Porous titanium manufactured by a novel powder tapping method using spherical salt bead space holders: Characterisation and mechanical properties

Jiangang Jia[a], Abdur R. Siddiq[b], Andrew R. Kennedy[b#]

[a] State Key Laboratory of Advanced Processing and recycling of Non-ferrous Metals, Lanzhou University of Technology, Lanzhou , China, 730050

[b] Manufacturing Research Division, Faculty of Engineering, University of Nottingham, University Park, Nottingham, NG7 2RD, UK

[#]*Tel: +44 115 9513744*

[#] *Email: andrew.kennedy@nottingham.ac.uk*

Abstract

Porous Ti with open porosity in the range of 70-80% has been made using Ti powder and a particulate leaching technique using porous, spherical, NaCl beads. By incorporating the Ti powder into a pre-existing network of salt beads, by tapping followed by compaction, salt dissolution and "sintering", porous structures with uniform density, pore and strut sizes and a predictable level of connectivity have been produced, showing a significant improvement on the structures made by conventional powder mixing processes. Parts made using beads with sizes in the range of 0.5-1.0 mm show excellent promise as porous metals for medical devices, showing structures and porosities similar to those of commercial porous metals used in this sector, with inter-pore connections that are similar to trabecular bone. The elastic modulus (0.86 GPa) is lower than those for commercial porous metals and more closely matches that of trabecular bone and good compressive yield strength is retained (21 MPa). The ability to further tailor the structure, in terms of the density and the size of the pores and interconnections has also been demonstrated by immersion of the porous components in acid.

1.0 Introduction

Permanent, porous biomaterial structures have the ability to provide a transitional space between bone and a biomaterial substrate (which provides the main structural support) and an appropriate level and geometry of porosity will allow the in-growth of new bone tissue and vascularisation, so that good integration with the host bone tissue can be obtained [1,2]. Porous titanium continues to attract attention as a biomaterial for medical applications, owing to its excellent specific mechanical properties, chemical stability and biocompatibility [1-3] and numerous processes have been developed to manufacture porous Ti, comprehensively reviewed in [2,4].

Porous metal fabrication using sacrificial space-holders offers the ability to control the pore size and shape, with the potential to achieve good pore uniformity and interconnectivity [5-10]. There are problems with this method, however, originating from unpredictable and inhomogeneous mixing of the space holder and

metal powder, exacerbated by irregularly-shaped space holders and powders with large differences in sizes. For these common cases, the homogeneity of space holder – metal powder blend is difficult to control, both within a part and from part-to-part. This is clearly unacceptable for a high quality product such as a medical device, which demands a robust and reproducible manufacturing route. Fig 1 shows examples of porous Ti structures made using space holders [7,10], exemplifying some of the problems, for example; irregular pore structures and struts of variable thickness, due to the use of irregularly-shaped space holders, and poor macro scale connectivity between pores, due to lack of space holder - space holder contact during the mixing process.

a)   b)
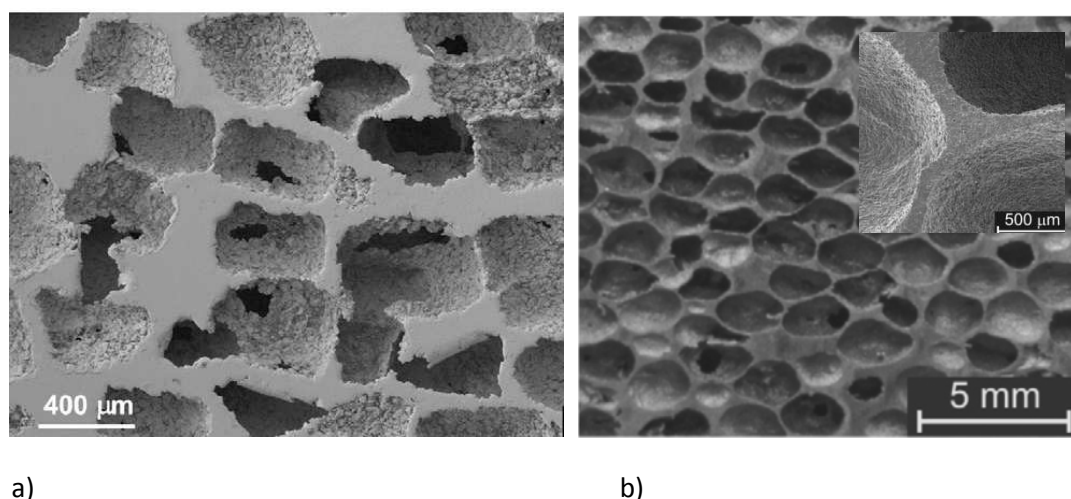
Figure 1 Porous Ti made using a space holder route showing (a) irregular pore structures [7] and (b) poor inter-pore connectivity [10]

This study aims to demonstrate a new approach to interspersing Ti powder with a spherical salt bead space holder, in an effort to enhance the reproducibility of mixing and hence of the porosity and interconnectivity in the resulting porous part. Porous Ti structures made by this route have been characterised and their structures and compressive mechanical properties are presented and compared with those for commercial porous metals used in medical devices.

2.0 Experimental

2.1 Materials

Commercial purity titanium powder with an irregular shape was used, as shown in Fig. 2, with a nominal size <45 μm (with a D_{50} of 39 μm with D_{10} and D_{90} values of 17 and 71 μm respectively). Near-spherical NaCl beads were produced according to a method described in [11] and were sieved into four different size ranges: 0.5-1.0 mm, 1.0-1.4 mm, 1.4-2.0mm and 2.0-2.5mm. The morphology of the smallest and largest NaCl beads in this range is shown in Fig. 3.

The packing behaviour for the two components was studied using a Quantachrome Autotap™ machine by tapping a known mass of powder in a graduated measuring cylinder. The apparent and tap densities were 0.90 and 0.97 g cc^{-1} for the salt beads (corresponding to packing fractions of 0.55 and 0.59 respectively for the porous NaCl beads, which have a density of 1.65 ± 0.05 g cc^{-1} [11]) and 1.47 and 1.98 g cc^{-1} for the Ti powder (corresponding to packing fractions of 0.33 and 0.44 respectively).

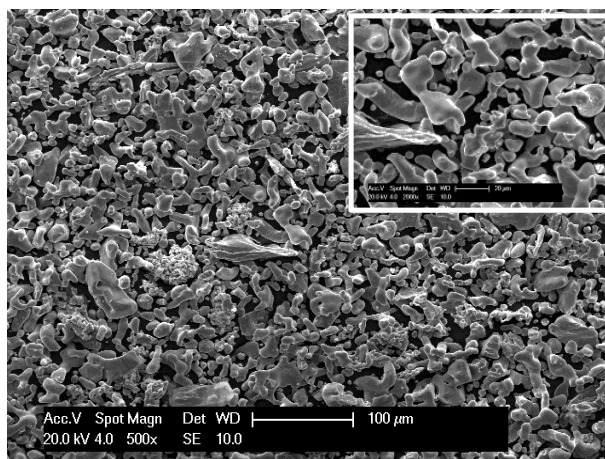Figure 2. SEM images of the titanium powder

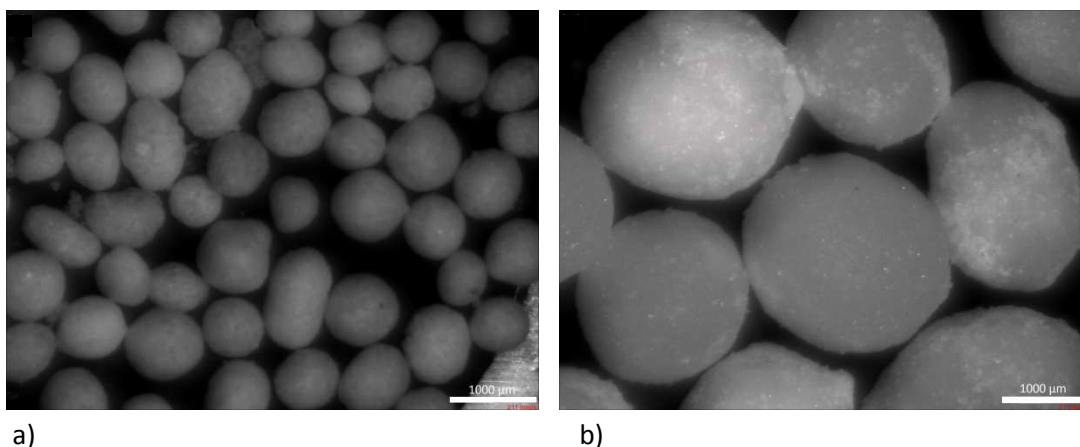a)   b)

Fig. 3 Optical micrographs of NaCl beads: (a) 0.5-1.0 mm, (b) 2.0-2.5 mm

2.2 Preparation of green parts

Ti powder and NaCl beads were combined using a tapping-based method similar to that reported in [12]. In this process, 4.3 g of salt beads were poured into the cavity of a 22 mm diameter die (with the bottom punch in place) and packing was enhanced by brief tapping using the same Autotap™ machine described earlier, which employs a simple lifting and dropping action, tapping at roughly 4 Hz. Ti powder, in varying masses (typically in the range of 2 to 4 g) was then placed on top of the bed, where after the top punch was inserted. The whole assembly was then tapped, using the same machine, stopping after a pre-determined

number of cycles. An image of the tooling and a schematic of the layered structure and the tapping direction (marked with an arrow) are given in Fig 4.

In order to track the progress of the Ti powder into the bed of beads, the distance that the top punch protrudes from the top surface of the die (shown in Fig 4) was measured as a function of the number of taps. Measurement was made by interrupting tapping and measuring the exposed height of the punch using a Vernier gauge with an estimated accuracy of ± 0.05 mm. With prior determination, in the same way, of the height of the bead bed (and how it varied with tapping), the height of the Ti layer above the bead bed could be estimated. The progression of the Ti powder through the bead of salt beads was also studied using X-ray micro-computed tomography (using a Scanco µCT 40 unit) by taking 2D radiographs and 2D horizontal sections of interrupted tapping experiments performed in an X-ray transparent Perspex^{TM} tube with a similar geometry to the die.

a)   b)
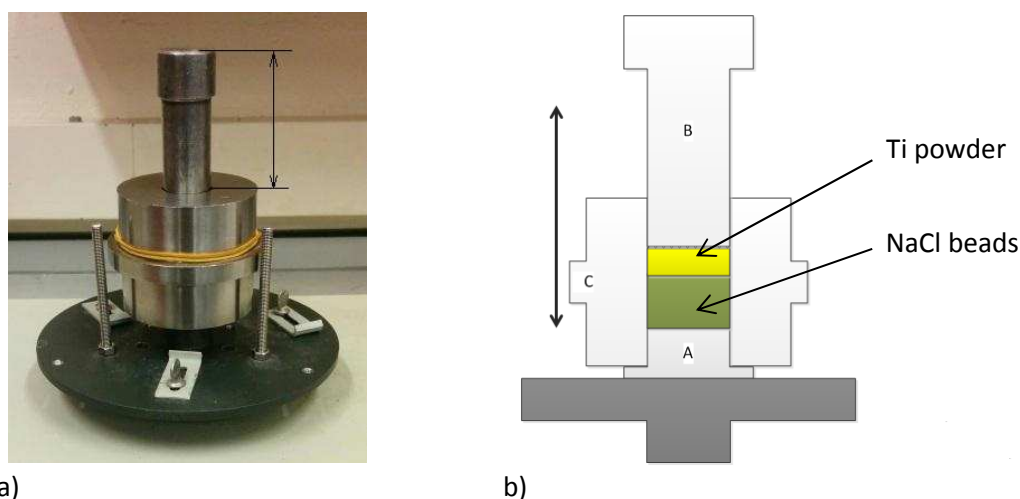
Figure 4: (a) Tapping tooling, showing the distance measured to determine the height of the punch in the die and (b) a schematic of the die including the powder layers (the arrow shows the tapping direction, A, B and C are the lower and upper punch and die respectively)

After interspersion by tapping, uniaxial die compaction was performed, at a pressure of 450 MPa, to produce robust Ti-NaCl "composite" pellets. The NaCl was removed before sintering by immersion in warm water, for up to 4 h and subsequent drying at a maximum of 90°C for a minimum of 3 h. Adopting this approach leads to a reduction in contamination of the sintering atmosphere compared with evaporation or burn-out during the sintering cycle (as is the case for polymer or carbamide space-holders).

For comparison, 0.5-1.0 and 1.4-2.0 mm NaCl beads were tumbled blended with the same Ti powder (at the same mass ratio as was found to be optimum for the tapping process) and further processed using the same methods as for tapped samples.

2.3 Sintering

The porous Ti parts were sintered in a tube furnace under an argon gas shield. Before heating, the tube was evacuated using a rotary pump and refilled with high purity argon, cycling through this process four times. With argon flowing through the tube at a rate of 100 ml min^{-1}, the Ti parts (resting on alumina substrates) were heated to 120°C at a rate of 5°C min^{-1} and held at this temperature for 30 min to remove any moisture. Thereafter the samples were heated to 1250°C at a rate of 5°C min^{-1} and held at this temperature for 3 h. The samples were then furnace cooled to room temperature. It should be noted that the sintering schedule was not optimised during this study.

2.4 Characterisation of porous titanium parts

The densities of porous samples were measured from their dimensions and mass. Green and sintered structures were sectioned through the height, using a cut-off wheel to minimise damage, and were ground and polished by hand, without water, on metallographic preparation wheels for observations using optical microscopy (OM) and scanning electron microscopy (SEM). Prior to inspection, any loose powder generated by cutting or grinding was removed by blowing with an aerosol air spray. X-ray micro-computed tomography (using a Scanco µCT 40 unit) was used to quantify features of the pore structure in sintered samples.

Compressive testing of porous structures was performed using an Instron 5969 Universal Testing machine, at a rate of 0.5 mm min^{-1}, compressing samples 22 mm in diameter, ground to 6 mm in height. In order to measure the stiffness, twin LVDT extensometers were used to accurately measure the compressive strain during multiple unloading and reloading cycles after initial loading to 75% of the compressive yield point (following a testing approach described in [13]).

3. 0 Results and discussion

3.1 General observations of the tapping behaviour

Loading the beads into the die, followed by tapping, creates a packed bed with a height of roughly 11 mm. This stable condition for the salt beads is achieved after fewer than 100 taps. Fig 5 shows the progressive change in height of the Ti layer on top of the salt bead bed with the number of taps applied, for a number of different NaCl / Ti mass ratios. What is immediately evident is that, as expected, the punch height decreases with tapping until a stable height is achieved. The number of taps required to achieve this stable condition decreases with increasing bead size (from roughly 2500 to 1200 taps for the smallest and largest beads respectively) indicating, as might be expected, faster migration of the Ti powder into larger inter-bead spaces.

These data have been used to try to determine the "optimum" mass of Ti for each bead size, assuming that a stable Ti layer height just greater than zero is required. It should be noted that although this may appear to be a rather crude measurement method, given the possibility of the bead packing fraction varying with extended tapping, results are strongly supported by visual evidence of either bead-rich or Ti-rich upper surfaces for both tapped and for subsequently compressed "composite" pellets. As an example, Fig 6 shows photographs of the surfaces of tapped samples, still in the die, that demonstrate the 3 conditions of; insufficient, near "optimum" and excess Ti additions.
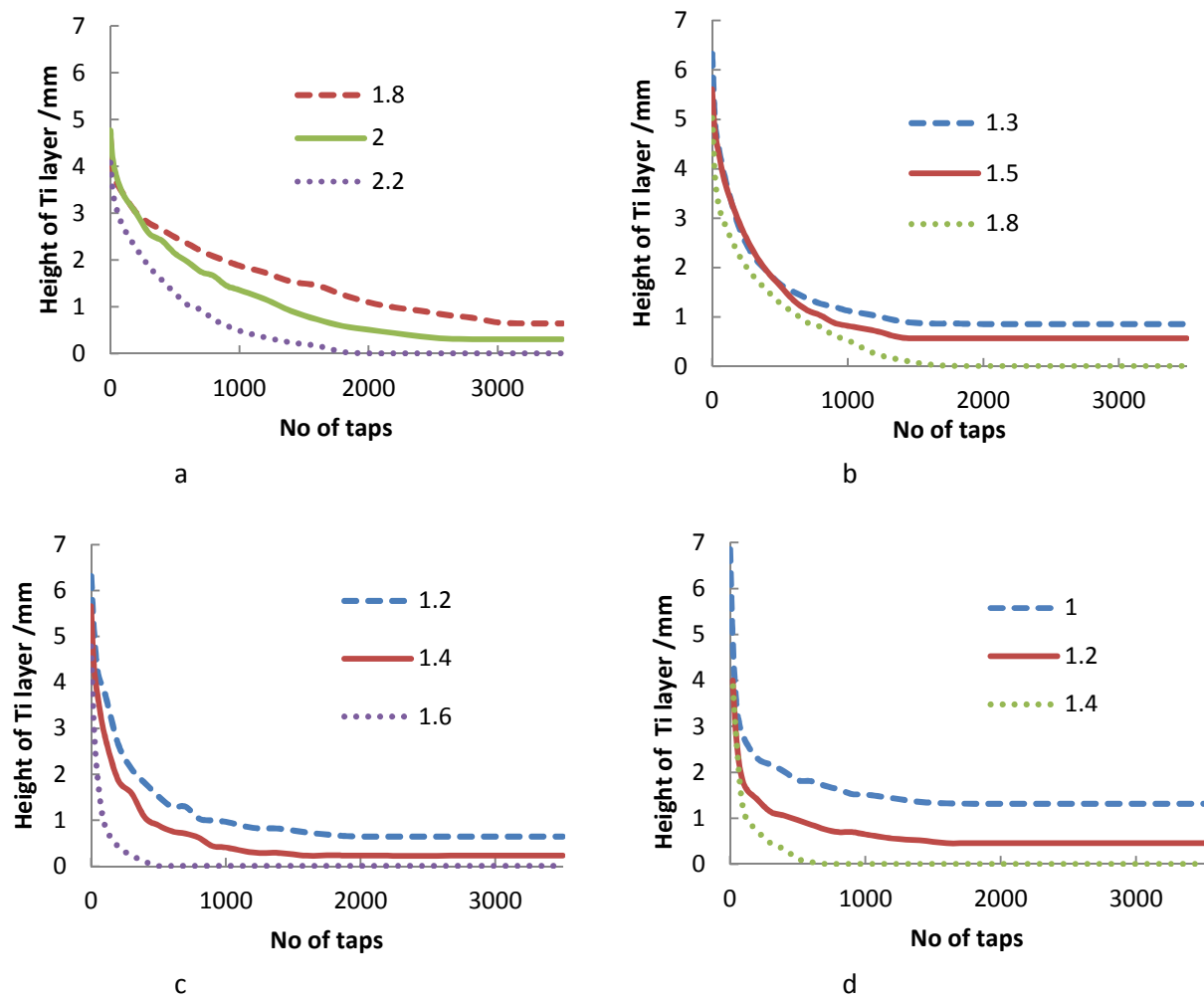
Fig. 5 Height of the Ti layer as a function of number of taps and NaCl / Ti mass ratio, for bead sizes of (a) 0.5-1.0 mm, (b) 1.0-1.4 mm, (c) 1.4-2.0 mm, (d) 2.0-2.5 mm (the nearest to optimum ratio is shown as a solid line)

Figure 6 Photographic images of the upper surface of tapped structures, in the die, showing (from left to right) insufficient, near "optimum" and excess Ti additions (for 1.4-2.0 mm beads)

6

The optimum mass ratio (of NaCl to Ti) decreases with increasing bead size (decreasing from 2.0 to 1.5, 1.4 and 1.2) indicating that despite the packing fraction of the beads remaining unchanged, more Ti can be accommodated in the network of beads as the bead size increases. This is a result of the decreasing fraction of small, impenetrable inter-bead spaces with increasing bead size. From the optimum mass ratios and the packing fraction for the beads, the packing fraction for Ti within the inter-bead locations can be estimated. As the bead size increases, the estimated packing fraction increases from 0.26 to 0.35, 0.39 and 0.42 respectively, values that are still below those for Ti tapped in an "infinite" vessel (0.44).

X-ray radiographs of vertical sections, in Fig 7, show the progression of the Ti powder (bright) from its initial position on top of the bead bed (for 0 taps the bead bed is 14 mm high and the Ti bed is 5 mm high), through the beads (for 50 taps the bead bed is 14 mm high and the Ti bed is 3 mm high) until it completely penetrates the bed (for 400 taps the total bed height is 14.5 mm). 2D horizontal sections, shown in Fig 8, taken at the same position, roughly 2 mm from the base of the vessel, show the preferential migration of Ti powder (bright) down the sides of the vessel, leaving unfilled pores (dark) between beads in the central region. The inter-bead voids in the centre, at the base, were always observed to be the last to fill and their location supports DEM simulations for the movement of tapped powder [14] which show fast migration from top to bottom via the side walls and slow movement from the outside to the centre. It should be noted that although the mechanism for Ti movement through the bead bed is unlikely to be altered by the die material used, Ti migration in the X-ray transparent Perspex[TM] vessel was found to be more rapid than in the heavier steel die.
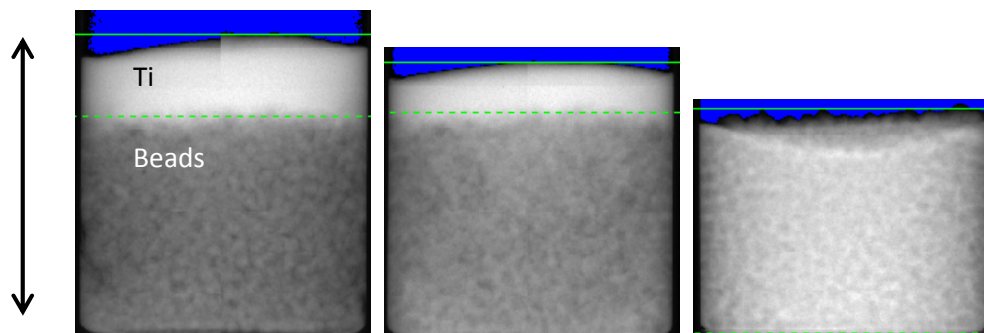

Figure 7 X-ray radiographs (for a Perspex[TM] tapping vessel) showing Ti (bright) migration for (from left to right) 0, 50 and 400 taps. The tapping direction is shown with an arrow.
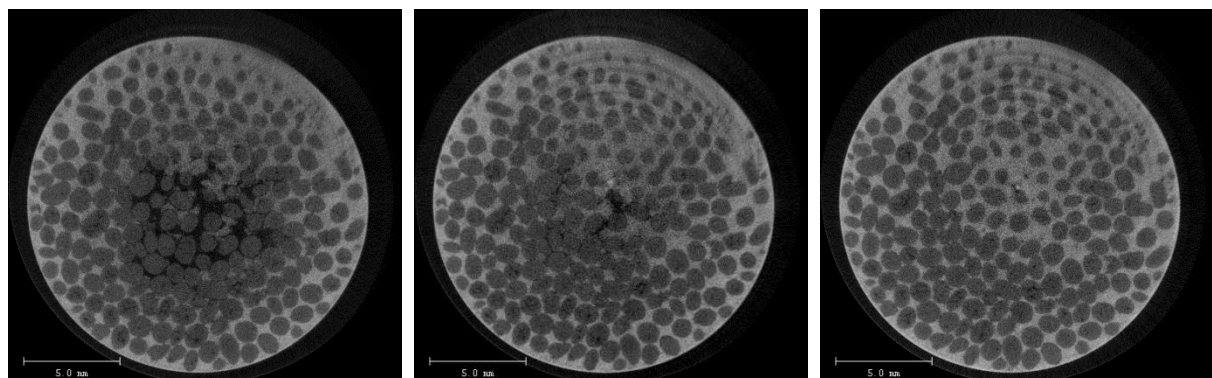
Figure 8 2D horizontal sections, 2 mm from the base of the Perspex™ tapping vessel after (from left to right) 50, 100 and 400 taps.

3.2 Green samples

Compaction resulted in a decrease in height of the samples to roughly 7 mm. By comparing the measured densities for the NaCl-Ti "composites" with those for the theoretical maximum density, from the densities and volume fractions of the constituents, it was apparent, in all cases, that compaction affected near-complete densification of the porous salt beads.

Samples for subsequent characterisation and testing were made using the "optimum" mass ratios previously established, removing, where necessary, any small layer of excess Ti from the top surface by light manual grinding. After the removal of excess Ti from the surface, and the NaCl, the porosities for bead sizes ranging from 0.5 to 2.0 mm were found to be 82, 79, 78 and 76% respectively, reflecting the less efficient filling of the inter-bead spaces for beds made from smaller beads.

Fig 9 shows vertical sections through green compacts after removal of the salt beads (with the compaction direction shown by the arrow). The structures observed are typical of porous materials made by this route, with uniform pore sizes and structures owing to the use of a narrow size range of near-spherical beads. Sectioning in this way shows that the pores have been flattened by the compaction process to become elongated perpendicular to the compaction direction, affected by the compressible nature of the beads. The aspect ratios for the beads are approximately the same for all bead sizes and correspond closely with the compression ratio (the ratio of the tapped height to the compressed height of the sample). It is also clear that there are multiple small windows linking adjacent pores and that this connectivity, in terms of the size and number of windows, is similar from pore-to-pore, throughout the structure. The number of connections, and hence windows per pore, is dictated by the coordination number for bead packing, which is, on average, between 5 and 6 for loose and dense random packing of spheres [15,16,17] and in broad agreement with observations. Measurement of the window size indicates that they increase with increasing bead size (from roughly 190 to 350 μm for the smallest and largest beads respectively) but that the ratio of window to bead size decreases as the bead size increases. The connections between pores are formed due to the inability of the Ti powder to penetrate the regions between and in the vicinity of neighbouring salt beads. The size of the resulting window will depend on the size of the Ti powder relative to the size of the beads, with larger windows expected, and observed, as the Ti powder is less able to pack into the inter-bead spaces as the beads reduce in size. The limited ingress of Ti powder into the small spaces between the salt beads is likely to result in an increasing frequency in the appearance of incomplete struts in samples made from smaller beads, either as a result of the lack of filling or due to the fracture of weak, thin struts during sectioning.

Fig 10 shows cell wall structures for green compacts made using 0.5-1.0 mm beads, where it is apparent that mechanical interlocking of the tapped and pressed, irregular Ti powder is capable of producing thin, self-supporting structures. This type of powder morphology is critical to the success of this process, as extensive collapse of porous structures was observed when dissolving salt from parts made using Ti with a more spherical morphology, even for very high compaction pressures (up to 700 MPa).
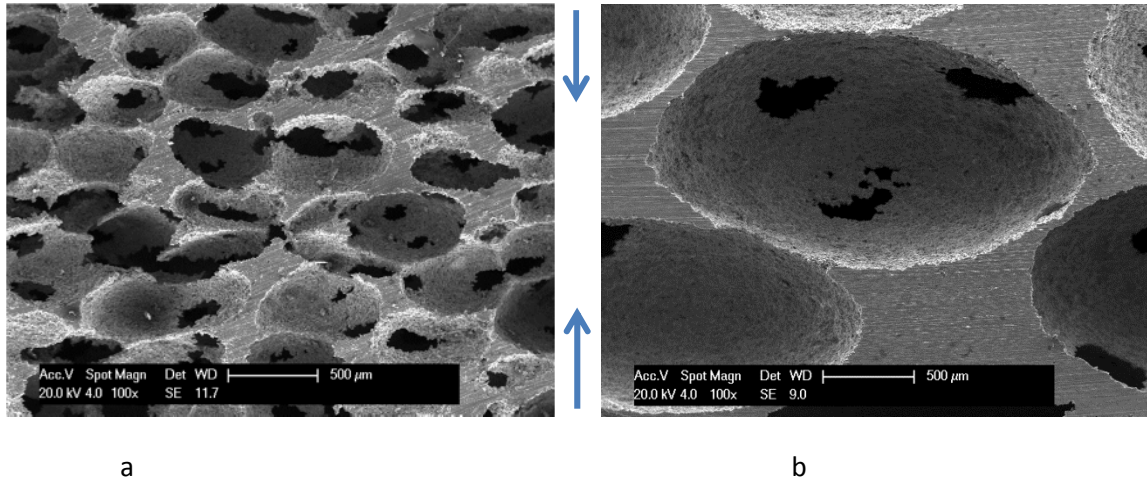
a   b

Figure 9 SEM images of vertical sections of green compacts with bead sizes (a) 0.5-1.0 mm, (d) 2.0-2.5 mm
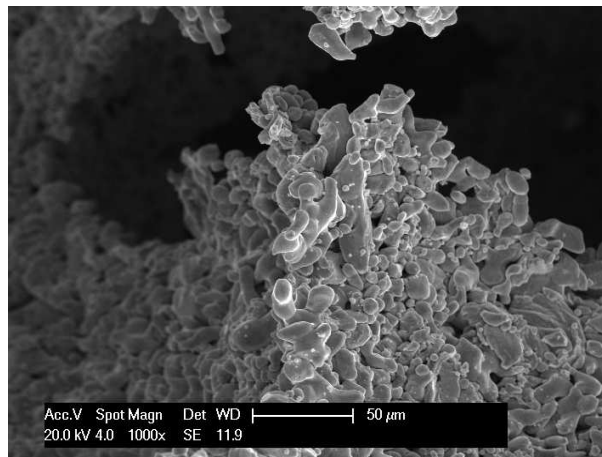(compaction direction is shown by the arrow)

Figure 10 SEM image of cell wall structure for a green compact made using 0.5-1.0 mm beads

3.3 Sintered structures

Fig 11 shows images of sintered samples for each bead size. It shows that sintering was successful and that significant warping or cracking was avoided. Shrinkage was of course observed, with volumetric reductions between 4-7%, leading to final porosities of 79, 75, 74 and 71% for samples made from 0.5-1.0 through to 2.0-2.4 mm beads. SEM images in Fig 12 show that the pore structure has been preserved through the sintering process and Fig 13 that sintering has resulted in densification of the cell walls, albeit with some residual porosity (which it might be possible to reduce with an optimised sintering schedule).
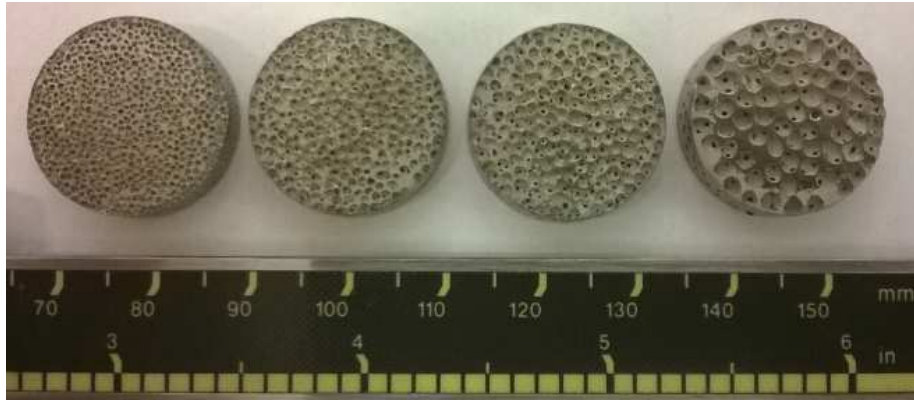
Figure 11 Images of sintered samples with increasing bead size (from left to right)
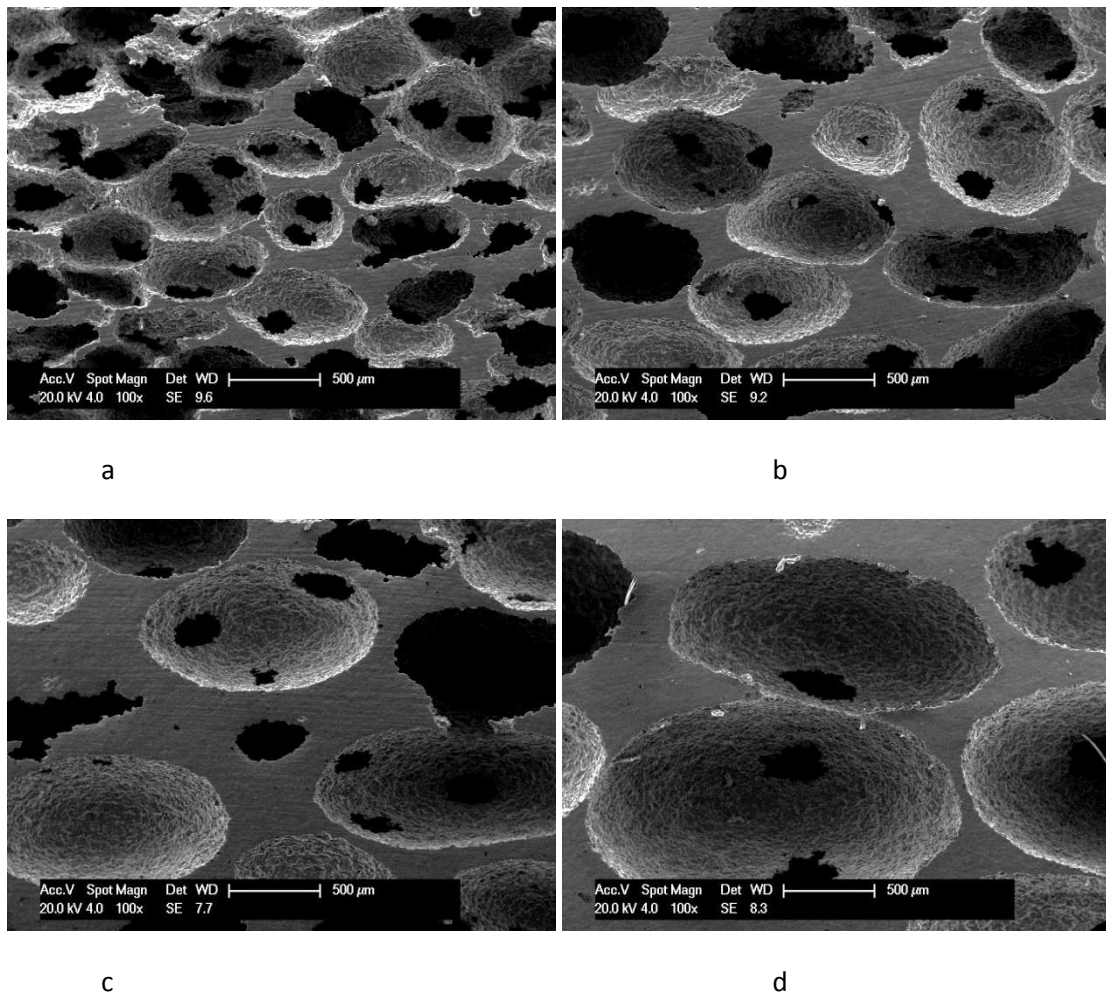

a

b

c

d

Figure 12 SEM images of vertical sections of sintered compacts with bead sizes (a) 0.5-1.0 mm, (b) 1.0-1.4 mm, (c) 1.4-2.0 mm, (d) 2.0-2.5 mm
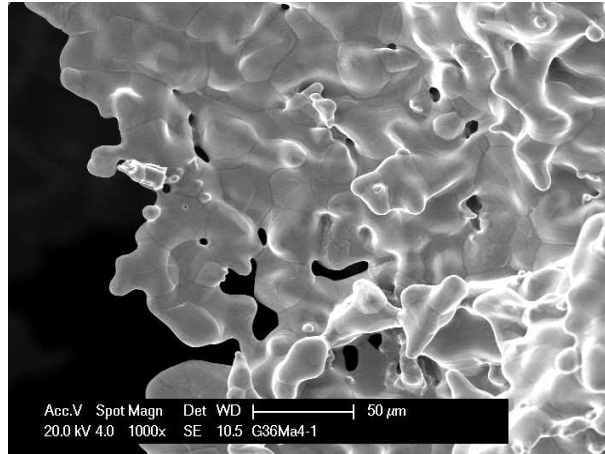
Figure 13 SEM image of cell wall structure for a sintered sample made using 0.5-1.0 mm beads

3.4 Comparison with conventional mixing

Figs 14 and 15 show optical and SEM images respectively, for sintered samples made by simple dry mixing and compaction of Ti powder and 0.5 - 1.0 and 1.4 - 2.0 mm beads (using the optimum mass ratio as defined earlier). It is clear that extensive collapse has occurred and although the images in Fig 14 are for sintered samples, collapse was observed after salt removal. The SEM images in Fig 15 clearly show less regular structures (than in Fig 12) with fewer and less well defined connections between the pores. This is even more apparent for the larger beads where a high level of retained salt was observed after dissolution (causing contamination of the tube furnace during the sintering step). The poor quality of the resulting structures is due to the inhomogeneous mixing of the two components, where Ti powder which completely surrounds the salt beads leads to a lack of connectivity, and localised clustering of NaCl beads results in Ti-depleted regions which are too weak to be self-supporting once the salt is removed. Mixing homogeneity is expected to be poor for a particle size ratio (NaCl / Ti) of nearly 20 for the smallest beads and worse still for the larger size differences present when using larger beads.
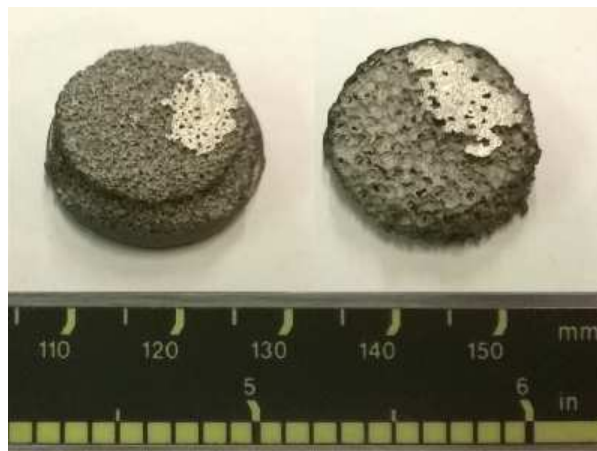

Figure 14 Images of porous (sintered) samples made by dry mixing using (left) 0.5-1.0 mm beads and (right) 1.4-2.0 mm beads
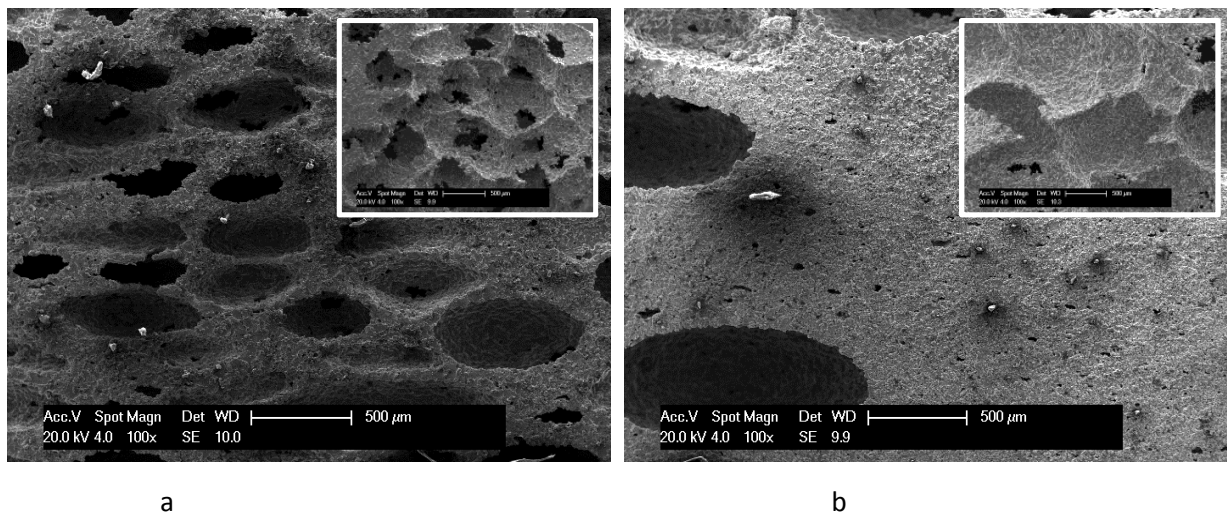
<div align="center">a   b</div>

Figure 15 SEM images of compacts made by dry mixing using (a) 0.5-1.0 mm and (b) 1.4-2.0 mm beads

3.5 Benefits and limitations of the tapping process

The tapping process creates a stable and fairly densely packed NaCl bead structure before the Ti powder is introduced and then facilitates the migration of the (relatively) fine Ti powder through the network of channels between the beads. Using near-spherical beads with a reasonably tight size range results in a homogenous network that is highly unlikely to have inaccessible areas of clustered space holder (as is more likely to be the case for angular particles with a wide size distribution). The tapping process also pre-establishes the inter-particle contacts which are well-defined due to the repeatable and predictable packing characteristics for near-monosized spherical particles. This is in stark contrast to the highly variable quality of the mixing of powders with a large size difference and the segregation problems associated with flow and transfer of these mixtures. Although the use of binders to coat the NaCl beads with Ti can create improved distributions of the two powders, and may overcome segregation of the fine powder, it will prevent direct bead-bead contact and hence greatly reduce the interconnectivity.

What is apparent is that the tapping process, albeit slow, taking as long as 10 min, if allowed to achieve a stable condition facilitates the filling of the available space within the packed bed of beads with Ti powder. Reducing the number of tapping cycles does not result in part-filling of these spaces, but leads to completely unfilled inter-bead regions at the base and the centre of the sample, resulting in parts of an unacceptable quality. Excess Ti simply remains on the top surface above the "saturated" bed structure. The porosity in the final part (although altered by compaction and sintering) is, principally dictated by the packing behaviour of the beads and of the Ti (which is in turn affected by the size of the inter-pore spaces relative to the size of the Ti powder). The result of this is that the ability to vary the pore fraction, especially for a given bead size, is limited. In order to raise or lower the porosity for a given bead size, the size of the Ti powder would need to be varied.

It should be noted that a rigid network of NaCl beads could be formed by sintering or using water or steam to affect inter-particle bonding and then this structure could be transferred to the die. In both cases, fine Ti powder can be tapped through the resulting NaCl bead network, but preliminary studies by these authors

revealed no benefit in terms of improved product quality or enhanced filling rate that would justify the additional processes involved.

4.0 Characterisation of samples for potential use in medical devices

4.1 Introduction

Since the service requirements for medical devices vary significantly, there are no clear rules to facilitate the optimal design of implants or bone substitutes in porous materials. This said, there are some clear objectives and the design of an appropriate porous structure necessitates a balance between achieving sufficient strength and adequate (and appropriately-sized) pore spaces for bone in-growth. Whilst specific targets for optimum pore fractions and pore sizes for implant fixation via bone in-growth remain undefined [1,3], previous studies and commercial porous metals often mimic trabecular bone, with porosities generally in the region of 70 to 80% and mean pore diameters in the range of 400 to 700 μm [1]. Additionally, the elastic modulus of the porous structure should match that of human bone in order to alleviate stress shielding. Given the above, sintered porous Ti samples manufactured using 0.5 - 1.0 mm beads have been characterised more fully.

4.2 Structural characterisation

Important to the production of high quality medical devices is the ability to produce parts that exhibit homogeneous structures (most notably pore size and porosity) both from part-to-part but also within a single part. In order to evaluate both these aspects, 10 parts were made with the same batch of beads, following the same process. The mean porosity for the batch was 79% with a standard deviation of less than 1.5%, illustrating that the process, if tapping is allowed to proceed so that filling is complete, is reproducible and that minimal variation in porosity from part-to-part, even after compaction, dissolution and sintering, can be achieved.

Fig 16 presents a sectioned CT image of a sintered structure, along with the porosity distribution taken from area fraction data from circa 250 2D sections, enabling the distribution of porosity through the full height of the porous structure to be evaluated. For ease of interpretation the porosity has been normalised with respect to the mean value. The variation in porosity with height is small, with a standard deviation below 2%, demonstrating the homogeneity of porosity within the sample, a result of the uniform packing of the beads and the uniform filling of the inter-bead spaces with Ti powder.
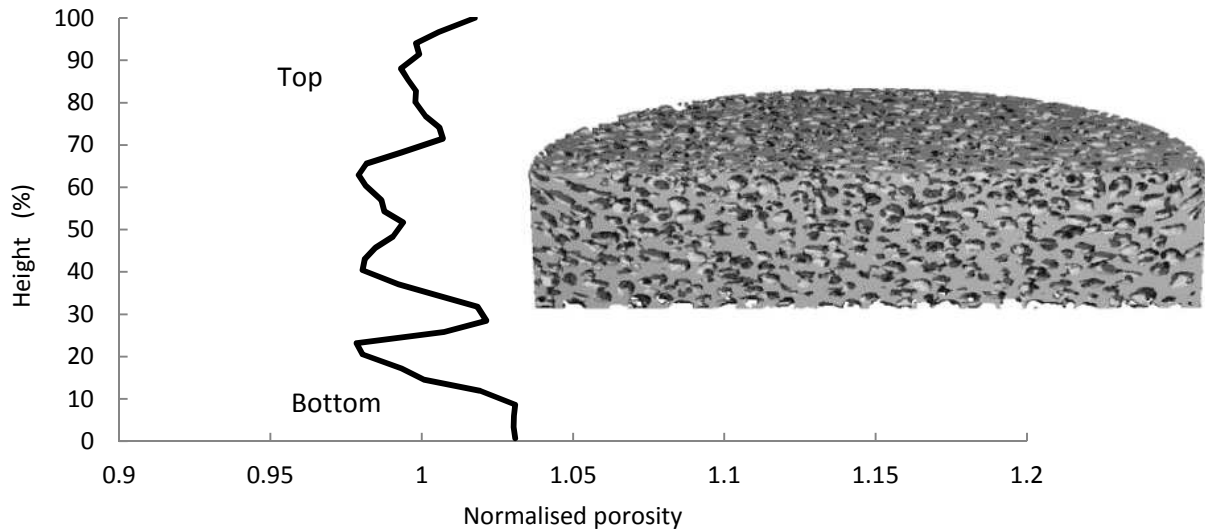
Figure 16 Normalised 2D porosity distribution as a function of height for a sintered sample made using 0.5-1.0 mm beads and corresponding CT image

Table 1 presents the structural characteristics for porous Ti parts and the measurement method is also shown. The mean pore diameter was measured (by CT) to be 375 μm with a standard deviation of 94 μm. This pore size measurement does not correspond closely to the bead size (0.5-1.0 mm) and this discrepancy is a result of both changes in the bead shape due to compaction and the technique used by the CT image processing software to quantify the pore size. The pore size is determined by filling the pores with the largest sphere possible, which for the compacted beads, which produce pores with an oblate spheroid shape, will approximate to the minor (z) axis. The degree of anisotropy, measured by CT, is approximately 1.6, a significant deviation from the initial value of 1.1, and this change is affected by the compaction process (for which the compression ratio is also close to 1.6). Owing to the porous, compressible nature of the NaCl spheres, the compaction process is also able to reduce them in volume (by an estimated 20%). By considering the aspect ratio, the mean length of the major axis of the pores is estimated to be 600 μm, consistent with measurements made from SEM images.

The size of the windows connecting the pores was measured using SEM and image analysis and was found to be 190 ± 40 μm, exceeding the minimum 100 μm thought to be necessary for bone in-growth [1]. The standard deviation in the measured values is high, in part as a result of a variety of possible contact geometries between beads at the top and bottom of the size fraction, but also highlighting the difficulty in measuring holes when observed away from normal to the viewing axis. A simple geometrical model based on touching spheres [17] predicts the mean window size (using the mid-range sizes for the beads and Ti) to be roughly 210 μm, close to the measured value, and is expected to be an upper bound given the enhanced packing characteristics of the irregularly-shaped Ti powder. The connectivity density, which represents the ratio of the connecting holes, vertices (end points), and struts (bridges) in one unit volume, was also measured and was found to be 16 mm^{-3}. Human bone has a connectivity density less than 12 mm^{-3}, with a mean close to 7 mm^{-3} [18,19] and hence the connectivity in the porous Ti is broadly in-keeping with that expected for a material designed to resemble the structure of bone.

Table 1 Structural characteristics for porous Ti made using 0.5-1.0 mm beads

Property	Measured by	Value
Porosity (%)	Mass - volume	79 ± 1.2
Pore size (µm)	CT	375 ± 93[#]
Strut thickness (µm)	CT	198 ± 73
Window size (µm)	SEM	190 ± 40
Connectivity density (mm^{-3})	CT	16
Degree of Anisotropy	CT	1.59

[#] value for the minor (z) axis of the elongated pores

4.3 Compressive mechanical properties

Figure 17 presents a stress – strain curve for a porous Ti sample and is typical of the batch of samples tested, showing an initial linear section, followed by a flatter plateau-like region and finally by densification which commences at strains between 0.4 and 0.5. The inset in Figure 17 shows an example of the stress-strain data, with strain data from the LVDT used to calculate the stiffness. In accordance with the literature, the stiffness measured on the first excursion is lower (in this case by more than 50%) than those for subsequent loading or unloading cycles (which are all in agreement within 2%) and is a result of microplasticity (yielding of some of the struts) at stresses below the macroscopic plateau stress [13]. Whilst measuring the gradient from the second loading cycle is an established method for determining the stiffness, clearly this won't adequately define the in-service performance if a device is made and not pre-loaded before implantation. Whilst this may appear trivial, clarity in reporting the method used to measure the stiffness is required. For an additional comparison, measurement of the stiffness using displacement data from the cross head of the machine, yielded a value that was only 40 % of that measured from the LVDT data, indicating the importance of eliminating the influence of machine compliance from the strain measurement. Table 2 summarises the mechanical properties, expressing them as an average over the batch of (10) samples tested, in this case reporting the stiffness measured during the initial loading step, using strain data from the LVDT.
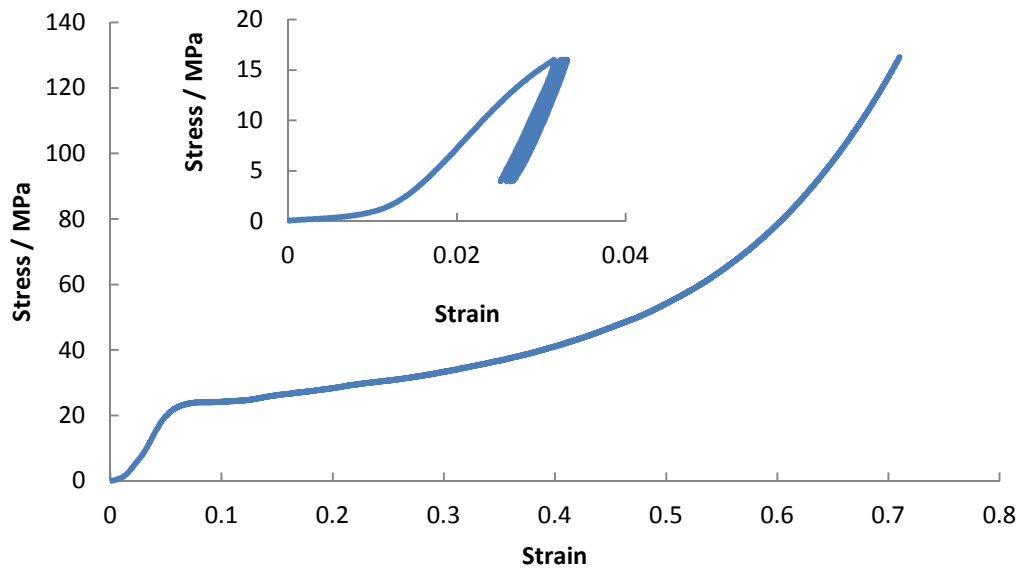
Figure 17 Typical stress-stain curve for a porous Ti structure made from 0.5-1.0 mm beads (inset, stress and strain data from the LVDT, used to measure the stiffness)

Table 2 Mechanical property data for porous Ti samples made from 0.5-1.0 mm beads

Porosity / %	RD	E / GPa	Yield Strength / MPa
79 ± 1.2	0.208 ± 0.002	0.86 ± 0.03	21.1 ± 1.8

The mechanical property data reported here lie within the broad scatter for the wealth of data reported for porous Ti [1] and match closely, in strength in particular, to porous Ti with similar structures and densities [20,21]. In addition to inappropriate testing methods and failure to meet the recommended condition that the sample height should exceed 7 times the mean pore diameter [13], deviations in reported properties, in stiffness in particular, also result from differing levels of cell wall porosity and contamination obtained during the differing sintering methods employed. A detailed comparison of structure and properties with porous Ti in the literature is avoided in favour of a comparison with those for commercial porous metals, presented in table 3 (taken from [1]) and trabecular bone [1,21]. Whilst the pore sizes and densities for the commercial porous metals closely mimic those of trabecular bone, the strength and stiffness exceed those of trabecular bone by some margin. For the material developed in this study, the stiffness is somewhat lower, most likely due to the higher level of porosity present in the cell walls, matching that of trabecular bone more closely, whilst still retaining good strength.

Table 3 Comparison of structural and mechanical properties of commercial porous metals and trabecular bone with porous Ti made in this study (after [1,20]).

	Biofoam[TM]	Regenerex[TM]	Trabecular Metal[TM] (Ta)	This Study	Trabecular bone

Total porosity (%)	60–70	67	75–85	79	70-80
Pore size (μm)	478–578	100–600	550	370-600[#]	400-700
Modulus (GPa)	2.5–3.0	1.6	2.5–3.9	0.86	0.05–0.5
Yield strength (MPa)	55–70	-	35–51	21	2–12

[#] the range given describes the minor and major axes for the ellipsoidal pores

4.4 Structural modification

Whilst for a given NaCl bead and Ti powder size the tapping process does not enable much scope for variation of some of the structural parameters, for example porosity and window size, the structure and porosity can be modified by simple immersion in acid to dissolve the thin Ti ligaments. An example of this process has been shown for samples immersed for 3 min in a 2% HF, 20% HNO_3 solution. From the mass change, the density decreased from 0.96 to 0.70 g cc^{-1}, increasing the porosity from 79 to 84%. SEM images in Fig. 18 compare structures before and after acid treatment, showing an "opening" of the structure. The structural changes were quantified using CT and plots for the pore size before and after etching are shown in Fig 19. This plot shows a shift in the pore size distribution to higher values and an increase in the mean pore size to 453 ± 117 μm. The window sizes were measured by SEM and were found to have nearly doubled to 374 ± 53 μm and the strut thickness decreased to 179 ± 79 μm. In the context of bone mimicry, the connectivity density improved, decreasing to 7.5 mm^{-3}. A reduction in density will, of course, be accompanied by a reduction in stiffness and strength. Although only measured for 3 samples, the mean stiffness and strength decreased to 0.55 GPa and 9.5 MPa respectively.
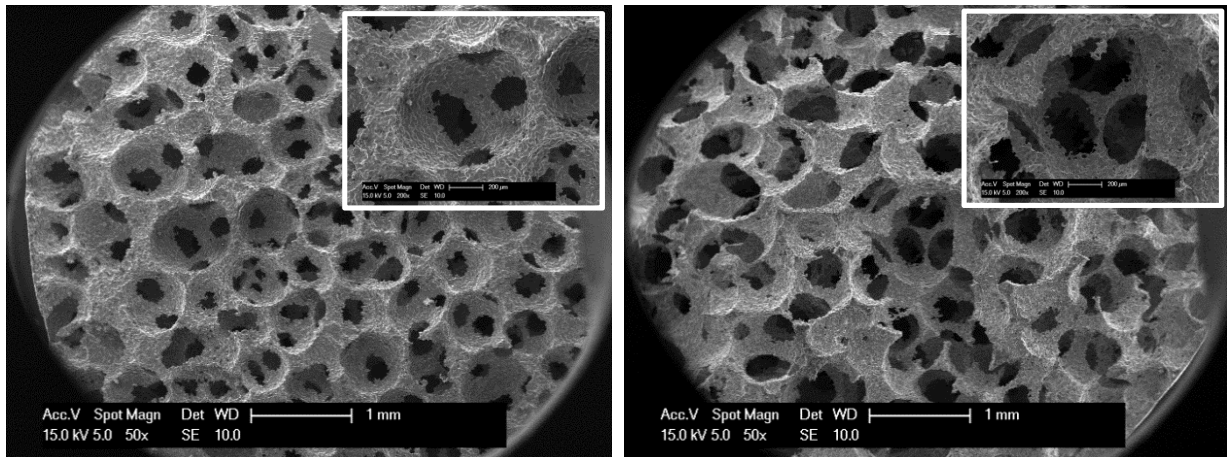

Figure 18: Horizontal sections of (different) porous Ti samples (left) before and (right) after acid etching in 2% HF, 20% HNO_3 for 3 min
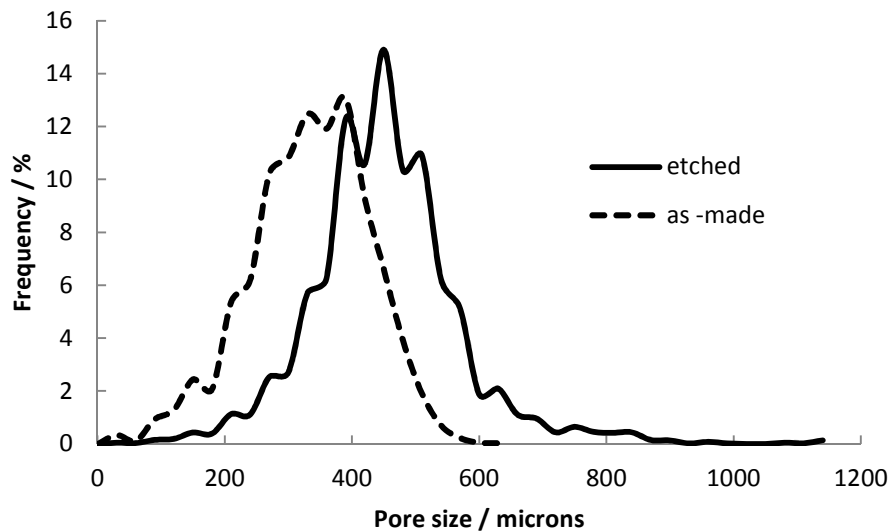
Figure 19 Pore size distributions for as-sintered and etched samples made using 0.5-1.0 mm beads

5.0 Summary

Porous Ti with open porosity in the range of 70-80% has been made using Ti powder and a particulate leaching technique using porous, near-spherical, NaCl beads. By incorporating the Ti powder into a pre-existing network of salt beads, by tapping followed by compaction, salt dissolution and "sintering", porous structures with uniform density, pore and strut sizes and a predictable level of connectivity have been produced, showing a significant improvement on the structures made by conventional powder mixing processes.

The migration and packing of the Ti powder within the network of beads has been studied, showing that migration is faster and packing is denser for networks of larger beads. The tapping process is, however, rather slow and can only be stopped after complete filling is achieved if robust, defect-free parts are to be produced. Whilst this does not allow the porosity to be varied for a particular metal powder – bead size combination, is does mean that if filling is complete, the variation in porosity from part-to-part is small and thus the process lends itself to the production of the high quality, reproducible structures that are required for medical devices.

Parts made using beads with sizes in the range of 0.5-1.0 mm show excellent promise as porous metals for medical devices, exhibiting structures and porosities similar to those of commercial porous metals used in this sector, with inter-pore connections that are similar to trabecular bone. The elastic modulus (0.86 GPa) is lower than that for commercial porous metals and more closely matches that of trabecular bone, which will help to reduce stress shielding, and good compressive yield strength is retained (21 MPa). The ability to further tailor the structure, in terms of the density and the size of the pores and interconnections has also been demonstrated by immersion of the porous components in acid.

References

[1] Gladius Lewis. Properties of open-cell porous metals and alloys for orthopaedic applications. J Mater Sci: Mater Med (2013) 24: 2293-2325;. doi: 10.1007/s10856-013-4998-y.

[2] Yuhua Li, Chao Yang, Haidong Zhao, Shengguan Qu, Xiaoqiang Li and Yuanyuan Li. New Developments of Ti-Based Alloys for Biomedical Applications. Materials 2014, 7, 1709-1800; doi: 10.3390/ma7031709

[3] M. Geetha, A.K. Singh, R. Asokamani, A.K. Gogia. Ti based biomaterials, the ultimate choice for orthopaedic implants – A review. Progress in Materials Science 54 (2009) 397–425.

[4] Garrett Ryan, Abhay Pandit, Dimitrios Panagiotis Apatsidis Fabrication methods of porous metals for use in orthopaedic applications Biomaterials 27 (2006) 2651–2670

[5] Z. Esen, Ş. Bor. Processing of titanium foams using magnesium spacer particles. Scripta Materialia . 56 (2007) 341-344

[6] Sung Won Kim, Hyun-Do Jung, Min-Ho Kang, Hyoun-Ee Kim, Young-Hag Kon, Yuri Estrin. Fabrication of porous titanium scaffold with controlled porous structure and net-shape using magnesium as spacer. Materials Science and Engineering C. 33 (2013) 2808-2815.

[7] Bing Ye, David C. Dunand. Titanium foams produced by solid-state replication of NaCl powders. Materials Science and Engineering A. 528 (2010) 691-697.

[8] Amirhossein Mansourighasri, N. Muhamad, A.B. Sulong. Processing titanium foams using tapioca starch as a space holder. Journal of Materials Processing Technology 212 (2012) 83– 89

[9] M. Sharma, G.K. Gupta, O.P. Modi, B.K. Prasad, Anil K. Gupta. Titanium foam through powder metallurgy route using acicular urea particles as space holder. Materials Letters 65 (2011) 3199–3201

[10] O. Smorygo, A. Marukovich, V. Mikutski, A.A. Gokhale, G. Jagan Reddy, J. Vinod Kumar, High-porosity titanium foams by powder coated space holder compaction method, Materials Letters 83 (2012) 17–19

[11] Jinnapat, A, *The manufacture and characterisation of aluminium foams made by investment casting using dissolvable spherical sodium chloride bead preforms*, in PhD Thesis, *Department of Mechanical, Materials and Manufacturing Engineering*. 2011, University of Nottingham

[12] A. Jinnapat, A.R. Kennedy. The manufacture of spherical salt beads and their use as dissolvable templates for the production of cellular solids via a powder metallurgy route. Journal of Alloys and Compounds 499 (2010) 43–47

[13] E.W. Andrews, G. Gioux, P. Onck, L.J. Gibson Size effects in ductile cellular solids. Part II: experimental results, International Journal of Mechanical Sciences 43 (2001) 701-713

[14] A Jain, M J Metzger, B J. Glasser, Effect of particle size distribution on segregation in vibrated systems, Powder Technology, Volume 237, March 2013, Pages 543–55

[15] Jerier, J.-F., et al., *Packing spherical discrete elements for large scale simulations.* Computer Methods in Applied Mechanics and Engineering, 2010. **199**(25–28): p. 1668-1676.

[16] Van Antwerpen, W., C.G. Du Toit, and P.G. Rousseau, *A review of correlations to model the packing structure and effective thermal conductivity in packed beds of mono-sized spherical particles.* Nuclear Engineering and Design, 2010. **240**(7): p. 1803-1818.

[17] P Langston, A.R. Kennedy, *Discrete element modelling of the packing of spheres and its application to the structure of porous metals made by infiltration of packed beds of NaCl beads*, Powder Technology, Volume 268, December 2014, Pages 210–218

[18] Thomsen, J.S., J. Barlach, and L. Mosekilde, *Determination of connectivity density in human iliac crest bone biopsies assessed by a computerized method.* Bone, 1996. **18**(5): p. 459-465

[19] Kabel, J., et al., *Connectivity and the elastic properties of cancellous bone.* Bone. **24**(2): p. 115-120.

[20] R. Singh, P.D. Lee, J.R. Jones, G. Poologasundarampillai, T. Post, T.C. Lindley, R.J. Dashwood, Hierarchically structured titanium foams for tissue scaffold applications Acta Biomaterialia 6 (2010) 4596–4604.

[21] Sandra C. P. Cachinho, Rui N. Correia. Titanium scaffolds for osteointegration: mechanical, in vitro and corrosion behaviour. J Mater Sci: Mater Med (2008) 19:451–457.